

1 NEWTS1.0: Numerical model of coastal Erosion by 2 Waves and Transgressive Scarps

3 Rose V. Palermo^{1,2}, J. Taylor Perron³, Jason M. Soderblom³, Samuel P. D. Birch^{4,5}, Alexander G.
4 Hayes^{3,4}, Andrew D. Ashton^{6,5}

5 ¹ U. S. Geological Survey, St. Petersburg Coastal and Marine Science Center, St. Petersburg, Florida 33701, USA

6 ² MIT-WHOI Joint Program in Oceanography/Applied Ocean Science & Engineering, Cambridge and Woods Hole,
7 MA, USA

8 ³Department of Earth, Atmospheric and Planetary Sciences, Massachusetts Institute of Technology, Cambridge,
9 MA, USA

10 ⁴Department of Earth, Environmental, and Planetary Sciences, Brown University, Providence, RI, USA

11 ^{5,4}Department of Earth, Atmospheric and Planetary Sciences, Cornell University, Cambridge, MA, USA

12 ^{6,5}Department of Geology and Geophysics, Woods Hole Oceanographic Institution, Woods Hole, MA, USA

13 Correspondence to: Rose V. Palermo (rpalermo@usgs.gov)

14 Abstract: Models of rocky coast erosion help us understand the physical phenomena that control
15 coastal morphology and evolution, infer the processes shaping coasts in remote environments,
16 and evaluate risk from natural hazards and future climate change. Existing models, however, are
17 highly complex, computationally expensive, and depend on many input parameters; this limits
18 our ability to explore planform erosion of rocky coasts over long timescales (100s to 100,000s
19 years) and a range of conditions. In this paper, we present a simplified cellular model of coastline
20 evolution [in reef closed basins](#) through uniform erosion and wave-driven erosion. Uniform erosion
21 is modeled as a constant rate of retreat. Wave erosion is modeled as a function of fetch, the
22 distance over which the wind blows to generate waves, and the angle between the incident wave
23 and the shoreline. This reduced complexity model can be used to evaluate how a detachment-
24 limited coastal landscape reflects climate, sea level history, material properties, and the relative
25 influence of different erosional processes.

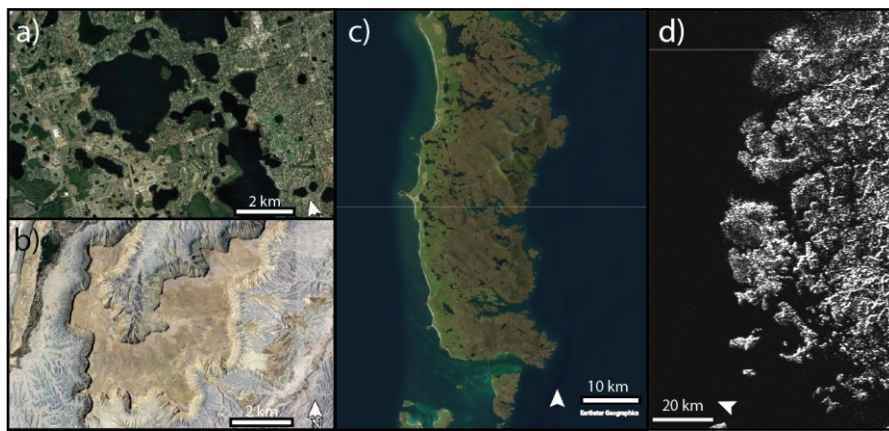
26 1 Introduction

27 Rocky coastlines are erosional coastal landforms resulting from the landward
28 transgression of a shoreline through bedrock. They make up approximately 80% of global coasts
29 (Emery and Kuhn, 1980) and often erode slowly through the impact of waves (Adams et al.,
30 2002, 2005), abrasion by sediment (Sunamura, 1976; Robinson, 1977; Walkden & Hall, 2005;
31 Bramante et al., 2020), and chemical weathering (Sunamura, 1992; Trenhaile, 2001). Rocky
32 coastlines protect coastal communities from erosion and flooding, provide sediment for estuaries,
33 marshes, and beaches, serve as important habitats (such as kelp forests), and support tourism
34 economies.

35 The imprint that each erosional mechanism leaves on the shoreline may be further
36 complicated by sea-level changes, accumulation and redistribution of sediment, heterogeneities
37 in the bedrock, or climate forcings. Wave-driven erosion occurs at a rate proportional to the
38 wave power (Huppert et al., 2020). Therefore, over long time scales, waves tend to erode more
39 exposed parts of coastlines preferentially, blunting headlands while preserving the shapes of
40 sheltered embayments. [South Uist, Scotland exemplifies this phenomenon, where the west side
41 of the island is open to the Atlantic Ocean and therefore smoother than the east side, which is
42 relatively protected \(Fig. 1c\).](#) Uniform erosional processes, like dissolution or mass backwasting,
43 erode at a nearly uniform rate everywhere along a coastline and result in smooth, rounded coastal

Formatted: English (United States)

44 features punctuated by skewed, pointy promontories or headlands (Howard, 1995). Instances of
45 dissolution and backwasting include karst lakes found in Florida, USA (Fig. 1a) as well as scarp
46 retreat due to weathering and backwasting, such as Caineville Mesa, Utah, USA (Fig. 1b).



48
49 Figure 16: a) Karst lakes in Florida, USA (Map Data: © Google Earth,
50 Landsat/Copernicus). Lake Butler and the surrounding region. b) Caineville Mesa, Utah, USA
51 (Map Data: © Google Earth, Landsat/Copernicus), c) South Uist, Scotland (Map Data: Esri
52 World Imagery, Earthstar Graphics). d) Cassini synthetic aperture radar (SAR) image of Kraken
53 Mare, Titan (NASA).

54
55 Although the relative influence of uniform erosion processes, such as dissolution, and
56 wave-driven erosion are still being quantified (Trenhaile, 2015), the shape of coastlines may
57 offer a means to infer dominant processes in remote environments where in situ measurements
58 are impractical. One such example are, such as arctic coasts, where local field data are sparse, or
59 remote planetary bodies, such as Titan (Fig. 1d). A reduced complexity model of long-term,
60 planform evolution of erosion-dominated coasts can provide insights about the importance of
61 wave erosion relative to uniform erosion, such as backwasting of permafrost (Günther et al.,
62 2013). Here, we present a reduced-complexity model of detachment-limited coastal erosion in
63 closed basins, such as lakes or inland seas, by uniform erosion and wave erosion. We test the
64 model by comparing our numerical solution of erosion with an analytical solution and test for
65 model result sensitivity to grid resolution and input parameters. Finally, we describe how this
66 model may be applied beyond closed basins to open coasts and islands (See Section 5).

67 2 Background

68 2.1 Previous Models of Coastal Erosion

69 2.1.1 Models of wave-driven erosion

70 Models of rocky-coastline geomorphology have historically focused on the erosion of the
71 cross-shore profile through sea-level rise (Walkden and Hall, 2005; Young et al., 2014), wave
72 impacts (Adams et al., 2002, 2005; Huppert et al., 2020), and the competing effects of sediment
73 abrasion and sediment cover (Kline et al., 2014; Young et al., 2014; Sunamura 2018; Trenhaile,
74 2019). But recent work has explored the alongshore variability (Walkden and Hall, 2005) and
75 planform evolution of these features (Limber & Murray, 2011; Limber et al., 2014; Sunamura,
76 2015; Palermo et al., 2021), with particular focus on either the relationship between planform
77 morphology and retreat rates following storms (Palermo et al., 2021) or the persistence of an
78 equilibrium coastline shape consisting of headlands interspersed with pocket beaches due to
79 variable lithology, grain size, or sediment tools and cover (Trenhaile, 2016; Limber & Murray,
80 2011; Limber et al., 2014).

81 Existing models of planform erosion of rocky beaches include 1) a mesoscale (1 to 100
82 years) alongshore-coupled cross-shore profile model, SCAPE (Walkden and Hall, 2005), in
83 which waves erode the substrate when the substrate is not armored by sediment and sediment is
84 transported by waves using linear wave theory; 2) a numerical model of sea-cliff retreat that
85 focuses on the mechanical abrasion of a notch at the cliff toe and subsequent failure of the cliff
86 and sediment comminution in the surf zone (Kline et al., 2014); and 3) a numerical model of
87 headlands and pocket beaches that takes into account wave energy convergence/divergence and
88 the processes of sediment production and redistribution by waves (Limber et al., 2014).

89 Previous work on marsh-shoreline erosion considers the heterogeneity of substrate
90 erodibility using a percolation theory model (Leonardi & Fagherazzi, 2015). In this system, low
91 wave energy conditions lead to patchy failure of large marsh portions, resulting in a strong
92 dependence on the spatial distribution of substrate resistance. In contrast, high-wave-energy
93 conditions cause the shoreline to erode uniformly, such that the spatial heterogeneity in marsh
94 erodibility does not influence the erosion rate (Leonardi & Fagherazzi, 2015). This ignores
95 variations in fetch, which can be important for rocky coastal systems.

96 These previous process-based models are all computationally expensive and require
97 specific knowledge of sediment and wave characteristics to accurately apply at local scales. To
98 model systems for which minimal field data are available, or to explore the general behavior of
99 planform erosion in rocky coasts under a broad range of conditions, a reduced-complexity model
100 (Ranasinghe, 2020) is necessary.

101 2.1.2+ Models of uniform erosion

102 ~~Shorelines formed by dissolution in karst landscapes have received some attention,~~
103 ~~mostly in the context of cave collapse features or sinkholes (Johnson, 1997; Martinez et al.,~~
104 ~~1998; Yechieli et al., 2006). However, most research has focused on the initial formation of these~~
105 ~~features; studies of the long term retreat of coastlines due to dissolution are focused on the~~
106 ~~meter scale erosion of coastal notches through mechanical and biochemical erosion and by~~
107 ~~dissolution (Trenhaile 2013; Trenhaile, 2015) and to our knowledge have not been evaluated~~
108 ~~over a larger spatial scale.~~

109 Howard (1995) modeled the retreat of a closed basin scarp as a uniform erosion process.
110 Howard's approach identifies gridded domain points as either interior or exterior to the
111 escarpment and erodes the escarpment edge at a constant rate in all directions originating from
112 adjacent points (Howard, 1995). In his model experiments, the escarpment retreats uniformly
113 toward the interior of the domain from the exterior. This uniform scarp retreat is analogous to
114 coastline retreat in response to dissolution of a uniform substrate. Although Howard's model was

15 designed for a different, subaerial system, uniform erosion of a ~~lake-closed-basin liquid~~ shoreline
16 can be described with the same process law, as we assume the planform ~~lake~~ shoreline also
17 erodes at the same rate in all directions.

18 Shorelines formed by dissolution in karst landscapes have received some attention,
19 mostly in the context of cave collapse features or sinkholes (Johnson, 1997; Martinez et al.,
20 1998, Yechieli et al., 2006). However, most research has focused on the initial formation of these
21 features: studies of the long-term retreat of coastlines due to dissolution are focused on the
22 meter-scale erosion of coastal notches through mechanical and biochemical erosion and by
23 dissolution (Trenhaile 2013; Trenhaile, 2015) and to our knowledge have not been evaluated
24 over a larger spatial scale.

26 ~~2.1.2 Models of wave-driven erosion~~

27 ~~— Models of rocky coastline geomorphology have historically focused on the erosion of the~~
28 ~~cross-shore profile through sea-level rise (Walkden and Hall, 2005; Young et al., 2014), wave~~
29 ~~impacts (Adams et al., 2002, 2005; Huppert et al., 2020), and the competing effects of sediment~~
30 ~~abrasion and sediment cover (Kline et al., 2014; Young et al., 2014; Sunamura 2018; Trenhaile,~~
31 ~~2019). But recent work has explored the alongshore variability (Walkden and Hall, 2005) and~~
32 ~~planform evolution of these features (Limber & Murray, 2011; Limber et al., 2014; Sunamura,~~
33 ~~2015; Palermo et al., 2021), with particular focus on either the relationship between planform~~
34 ~~morphology and retreat rates following storms (Palermo et al., 2021) or the persistence of an~~
35 ~~equilibrium coastline shape consisting of headlands interspersed with pocket beaches due to~~
36 ~~variable lithology, grain size, or sediment tools and cover (Trenhaile, 2016; Limber & Murray,~~
37 ~~2011; Limber et al., 2014).~~

38 ~~Existing models of planform erosion of rocky beaches include 1) a mesoscale (1 to 100~~
39 ~~years) alongshore-coupled cross-shore profile model, SCAPE (Walkden and Hall, 2005), in~~
40 ~~which waves erode the substrate when the substrate is not armored by sediment and sediment is~~
41 ~~transported by waves using linear wave theory; 2) a numerical model of sea-cliff retreat that~~
42 ~~focuses on the mechanical abrasion of a notch at the cliff toe and subsequent failure of the cliff~~
43 ~~and sediment comminution in the surf-zone (Kline et al., 2014); and 3) a numerical model of~~
44 ~~headlands and pocket beaches that takes into account wave energy convergence/divergence and~~
45 ~~the processes of sediment production and redistribution by waves (Limber et al., 2014).~~

46 ~~Previous work on marsh shoreline erosion considers the heterogeneity of substrate~~
47 ~~erodibility using a percolation theory model (Leonardi & Fagherazzi, 2015). In this system, low~~
48 ~~wave energy conditions lead to patchy failure of large marsh portions, resulting in a strong~~
49 ~~dependence on the spatial distribution of substrate resistance. In contrast, high wave energy~~
50 ~~conditions cause the shoreline to erode uniformly, such that the spatial heterogeneity in marsh~~
51 ~~erodibility does not influence the erosion rate (Leonardi & Fagherazzi, 2015). This ignores~~
52 ~~variations in fetch, which can be important for rocky coastal systems.~~

53 ~~— These previous process-based models are all computationally expensive and require~~
54 ~~specific knowledge of sediment and wave characteristics to accurately apply at local scales. To~~
55 ~~model systems for which minimal field data are available, or to explore the general behavior of~~
56 ~~planform erosion in rocky coasts under a broad range of conditions, a reduced-complexity model~~
57 ~~(Ranasinghe, 2020) is necessary.~~

158 3 Model

159 We developed the Numerical model of coastal Erosion by Waves and Transgressive
160 Scarps, V1.0 (NEWTS1.0) (Palermo et al., 2023) to study the planform-shoreline erosion of
161 detachment-limited coasts by waves, uniform erosion, or a combination of these processes. This
162 reduced-complexity model can be used to explore long-term (~~1000s yrs - 1 Myr~~thousands to
163 millions of years~~0,000s of years~~) trends in landscape evolution that result from these processes
164 across the appropriate sea- or lake- level change conditions. Uniform erosion includes
165 dissolution or mass backwasting and is modeled with a spatially uniform rate of shoreline retreat,
166 which generally smooths the coastline ~~but and~~ generates cusped points where promontories are
167 eroded. Wave erosion occurs in proportion to the wave energy that the coastline is exposed to
168 and to the angle of incidence of the incoming waves, such that the erosion rate depends on the
169 wave energy in the cross-shore direction per unit of length along the coast (Komar, 1997; Ashton
170 & Murray, 2009; Huppert et al., 2020). Coastlines that have larger exposure ~~to the lake~~ (larger
171 fetch) experience higher wave energy and therefore faster wave erosion. We model this energy-
172 dependent erosion by computing the fetch of every incident wave angle that may impact a given
173 point on the shoreline and weighting this fetch by the cosine of the angle between the incident
174 wave crests and the shoreline. Mathematically, this is equivalent to the dot product of the
175 direction of wave travel and the direction normal to the shoreline.

177 3.1 General description and model setup

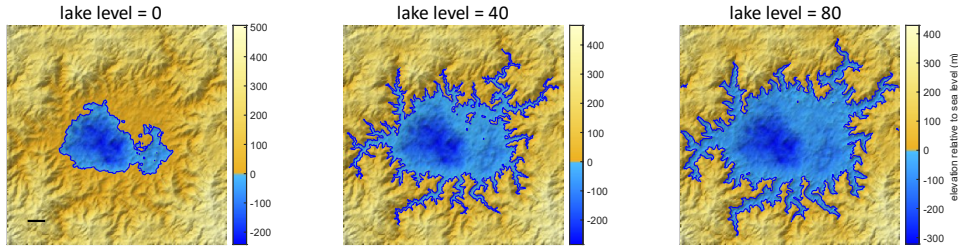
178 3.1.1 Model domain and structure

179 3.1.1.1 Model domain

180 The domain of the model (~~Fig. 1~~Fig. 2) is a grid discretized into N_x cells in the x direction
181 and N_y cells in the y direction, with cell spacings Δx and Δy , such that $x_i = i\Delta x$ and $y_j = j\Delta y$.
182 The value of each grid cell, $z_{i,j}$, corresponds to the landscape elevation. The boundaries of the
183 grid are periodic. Each cell in the domain is defined as either liquid or land based on its elevation
184 relative to sea or lake level. The model could apply to lake level in closed liquid bodies or sea
185 level in semi-closed seas or open coasts. For simplicity, in this manuscript we will use “lake” to
186 refer to the liquid bodies, “lake cell” refers to cells occupied by liquid, and “lake level” refers to
187 the elevation of the liquid level. Cells below ~~sea or lake~~ level are fixed and do not erode.
188 Shoreline cells, defined as land cells directly adjacent to liquid, may be eroded by coastal
189 processes through uniform erosion and wave erosion. L~~Sea or lake~~ level is an input to the system
190 that the user can vary throughout a model run.

191

192
193



194
195 Figure 24: Example model domain with a sea or lake level of a) 0 m, b) 40 m, and c) 80 m. This
196 domain is used in Figs. 4 and 5.

197 3.1.1.2 Identification of lake-liquid body and shoreline cells

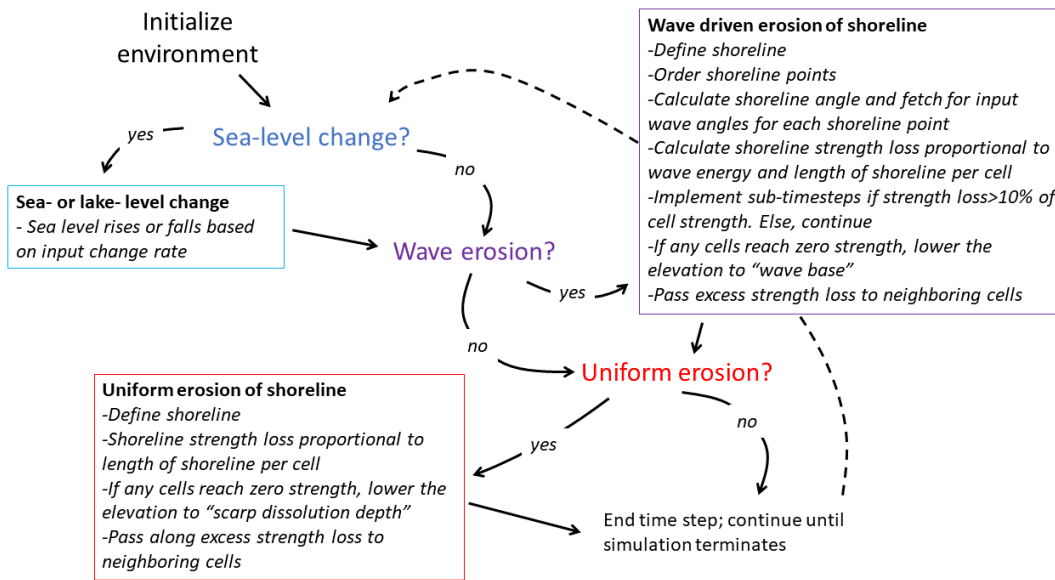
198 Boundaries in the grid are identified using pixel connection definitions of either 4-connected,
199 wherein which a-connections occurs only across any side-edges, or 8-connected, in which where a
200 connections occurs either across edges any side or vertex at corners. Liquid cells that are 8-
201 connected to each other comprise the same lake liquid body. The liquid body could represent an
202 sea or lake, so for simplicity we call a liquid cell a “lake cell” and a liquid body a “lake” in this
203 manuscript. Islands are defined as groups of land cells that are surrounded by liquid cells. Lakes
204 can also occur inside islands and islands inside these lakes, so we define a lake hierarchy to
205 identify and model each lake individually. The first level in this hierarchy is the land that is
206 connected to the border of the domain. First order lakes are lakes that are immediately
207 surrounded by this land that extends to the border of the domain. A first order island is
208 immediately surrounded by a first order lake. A second order lake is surrounded by a first order
209 island, and so on. This continues such that Nth-order islands are surrounded by Nth-order lakes,
210 and Nth-order lakes are surrounded by N-minus-one-order islands. This hierarchy allows us to
211 identify and isolate unique lakes, which will be important when we consider wave-driven
212 erosion.

213 214 3.1.1.3 Cellular grid erosion

215 Each cell starts with an initial strength, S_{init} , (see Sections 3.1.3 to 3.3) which is depleted
216 according to a rate law associated with each coastal process until reaching 0 (see Sections 3.2
217 and 3.3), at which point the cell erodes. Coastal erosion occurs on shoreline cells, defined as land
218 cells adjacent to liquid cells, and decreases the elevation of those cells by a specified depth of
219 erosion, d_e , which is user specified. For cells eroded by coastal processes, $\mathbf{z}(\mathbf{t}) = \mathbf{z}(\mathbf{t} - \mathbf{1}) -$
220 d_e , where \mathbf{t} is model time. For uniform erosion, d_e is conceptualized as the scarp dissolution
221 depth. For wave erosion, is conceptualized as a wave base. Shoreline cells become lake cells
222 once eroded. To avoid numerical artifacts associated with the time discretization, the timestep
223 must be set such that the amount of erosion per iteration is a small fraction of the total cell size.
224 In practice, we set the time step to erode less than $1/10^{\text{th}}$ of a cell at a given time given the cell
225 spacing and rate law. The model run terminates if a lake cell becomes adjacent to a boundary cell
226 because the wave erosion model requires a closed coastline.
227

228 3.1.1.4 Order of operations

229 During each timestep, erosion occurs according to three steps, if enabled: 1) Sea- or lake-
 230 level Change, 2) Wave Erosion, and 3) Uniform Erosion (Fig. 2 Fig. 3). Here we describe the
 231 general model components and simulation procedure. The governing equations for Uniform
 232 Erosion and Wave erosion are outlined in more detail in sections 3.2 and 3.3, respectively.
 233



234
 235 Figure 32: Model structure showing the time loop in which the model 1) updates sea- or lake-
 236 level change, then calculates shoreline erosion due to 2) waves and 3) uniform erosion processes.

237
 238 The first operation of the model is sea- or lake-level change. The sea- or lake-level changes as
 239 an input rate or according to an input sea- or lake- level curve. The new sea- or lake- level is used
 240 to define the lake(s) and shoreline(s) (Section 3.1.1.2 and 3.1.2).

241 Next, wave erosion of the shoreline(s) occurs as a function of the fetch—the open-water
 242 distance wind and waves travel before reaching a point on the coast—and the angle between the
 243 wave crests of the incident waves, ϕ , and the azimuth of the shoreline, θ (Section 3.3). In this
 244 module, the shoreline is first identified and traced such that shoreline cells are ordered in a
 245 counterclockwise direction. The shoreline is then used to calculate the shoreline angle, incident
 246 wave angle, and associated fetch at each cell along the shoreline (Section 3.3.1). The elevation of
 247 eroded shoreline cells is lowered, their labels are changed to liquid cells as appropriate, and the
 248 shoreline is updated (See Section 3.4, Fig 5). This approach considers sediment removal as
 249 instantaneous. Future variations of the model could consider the erosion also as a function of the
 250 height of the material being eroded or the excavation rate of weathered rubble.

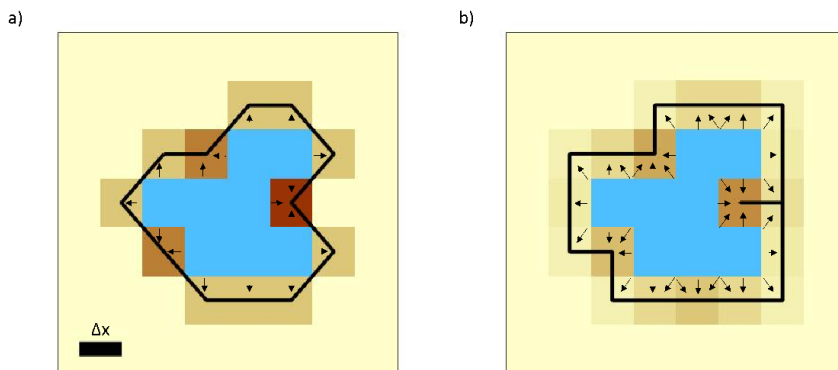
251 Finally, uniform erosion of the updated shoreline occurs (Section 3.2). Here, the shoreline
 252 erodes as a function of the alongshore length of the shoreline as measured along cell boundaries

253 (Section 3.1.2 and 3.2). And again, the elevation of eroded shoreline cells is lowered, the labels
254 of eroded cells are changed to liquid cells, and the shoreline is updated.

255
256 3.1.2 Defining the shoreline

257 There are two options for defining shoreline cells: ~~land cells that are either the 84~~-connected
258 ~~case, in which successive land cells along the shoreline may border one another either at cell~~
259 ~~edges or at cell corners to the lake liquid, where a land cell borders a liquid cell on any side (Fig.~~
260 ~~3Fig. 4a), or the 48~~-connected case, in which successive land cells along the shoreline may
261 ~~border one another only at cell edges to the lake liquid, where a land cell borders a liquid cell on~~
262 ~~any side or vertex (Fig. 3Fig. 4b). In the case of an 8-connected shoreline, shoreline cells only~~
263 ~~border liquid cells at cell edges (Fig. 4a), whereas shoreline cells in a 4-connected shoreline can~~
264 ~~border liquid cells at cell edges or at cell corners (Fig. 4b). We choose Δx and Δy to be small~~
265 ~~enough to represent the relevant features of the shoreline. If sea-or-lake-level change occurs in~~
266 ~~the simulation, the relevant features in the landscape should be taken into account when choosing~~
267 ~~Δx and Δy . Here, we present simulations where Δx and Δy are equal. The model can operate~~
268 ~~with different Δx and Δy ; however, there could be resulting differences in error which have not~~
269 ~~been tested.~~

Formatted: Indent: First line: 0"



270
271 Figure 43: Shoreline cells and associated strength loss weighting for a shoreline that is a) 84-
272 connected to liquid cells or b) 48-connected to liquid cells. Arrows point in the direction of
273 erosion into each shoreline cell from neighboring lake cells. Increasing darkness of shoreline
274 cells indicate increasing strength loss weighting.

275 The shoreline cells need to be ordered so that the lake can be represented as a polygon for
276 the fetch computation. To order the shoreline cells in closed loops, we start at the first indexed
277 shoreline cell of the longest shoreline and move counterclockwise to find the next shoreline cell.
278 Once a sequence of the first 3 cells is repeated, the loop is closed and the shoreline is deemed
279 complete. Any remaining shoreline cells that do not lie on this loop represent the shoreline of a
280 separate first-order lake, or of an island or higher order lake contained within the lake. Next,
281 ordering the shorelines of the islands contained within the current lake begins on the first
282 remaining shoreline cell. We repeat this process until all land cells bordering liquid are included
283 in a closed shoreline. When there are multiple first-order lakes in a landscape domain, the
284 shorelines for each lake and its enclosed islands are ordered one at a time.

285 3.1.3 Cell strength and coastal erosion processes

286 All cells start with an initial strength, S_{init} , which represents how difficult it is to erode
287 the land (Equation 1). We model the domain as having uniform strength [in both planform space](#)
288 [and elevation](#), but this could easily be extended to a scenario with heterogeneous strength. The
289 strength of a cell is initialized as a reference strength, S_0 , multiplied by the ratio between the cell
290 area, $A = \Delta x \Delta y$, and a reference cell area, $A_0 = \Delta x_0 \Delta y_0$, with reference spacing Δx_0 and Δy_0
291 (Equation 1). The reference strength and area nondimensionalize strength and maintain
292 proportions that mitigate discretization bias. The magnitude of these values can be chosen by the
293 user.

$$294 \quad S_{init} = S_0 \frac{A}{A_0} \quad (1)$$

295 Strength is lost from each shoreline cell at a rate that depends on the exposed perimeter of
296 the cell and an erosion rate law specific to either uniform erosion or wave erosion processes.
297 Change in strength is grid-independent for grids sufficiently fine to satisfy model stability
298 because the strength is initialized with a reference cell area in proportion to the parameterized
299 cell area. To mitigate discretization bias, Δx , Δy , and Δt must be sufficiently small that Δt is less
300 than the time to completely erode a cell (See Sections 3.2 and 3.3), and that Δx and Δy properly
301 represent the shoreline morphology. In practice, we choose Δx to be equal to Δy .

302 As time progresses, each shoreline cell loses strength until failure, $S_{i,j} = 0$, at which
303 point the cell has eroded. It is possible for the strength loss in one time step to exceed the
304 remaining strength of the cell. When this occurs, the excess time spent eroding the cell is passed
305 along to all new shoreline neighbors of the eroded cell, representing the time of erosion that
306 neighboring cell will incur after the erosion of the original shoreline. If a new shoreline cell is
307 inheriting excess time from multiple neighbors, the mean excess time is used to compute the
308 strength loss. In our simulations, taking the mean of the excess time resulted in the least grid
309 bias.

310 Modeled erosion could be underestimated or redistributed improperly if the strength loss
311 for an eroding cell is consistently large relative to the initial strength of the domain. The
312 shoreline would then not update with the newly exposed cells, rather constantly passing strength
313 loss to its neighbors, and inaccurately characterizing the morphology. We implement a sub-
314 timestep routine to capture the effect of the changing shoreline within a single timestep when the
315 strength loss of any shoreline cell in the domain exceeds a certain threshold of the initial
316 strength, α , which ranges between 0 and 1. In the modified time-step routine, the damage is

317 computed and the shoreline updated in sub-timesteps, which segments the time-step and allows
 318 erosion to occur in smaller increments.

319 3.2 Uniform erosion model

320 The rate of shoreline retreat by uniform erosion is set by an erodibility coefficient,
 321 $k_{uniform}$ (Eq. 2). Strength loss due to uniform erosion occurs as a function of the amount of
 322 shoreline in contact with the lake for a given cell, represented as the number of 4-connected
 323 sides, s , and 8-connected corners, c , in contact with lake cells (Eq. 3; ~~Fig. 3~~ Fig. 4). Because the
 324 diagonal of the cell is longer than the side by a factor of $\sqrt{2}$, it would take $\sqrt{2}$ times longer for a
 325 shoreline to retreat across a cell diagonal than in the perpendicular direction. To correct for this
 326 in our model, the strength loss computed from an exposed corner is $\sqrt{2}/2$ as much as the strength
 327 lost from an exposed side.

$$328 \quad \frac{dx}{dt} = k_{uniform}, \quad (2)$$

$$329 \quad \frac{\Delta S_{ij}}{S_0} = -k_{uniform} \left(s_c + \frac{\sqrt{2}c}{2} \right) \frac{\Delta x}{\Delta x_0} \Delta t, \quad (3)$$

330 3.3 Wave erosion model

331 Wave erosion occurs at a rate determined by a wave erodibility coefficient, k_{wave} [m·yr⁻¹],
 332 and the wave energy flux in the cross-shore direction, E (Eq. 4). The wave energy flux
 333 depends on the wave height, H , and the angle between the wave crests of the incident waves, φ ,
 334 and the azimuth of the shoreline, θ (Eq. 5). Wave height scales with fetch, F , such that $H \propto \sqrt{F}$
 335 (Hasslemann, 1973; Smith and Waseda, 2008). Therefore, we use fetch to approximate the wave
 336 energy density for a wave from a given direction on a coastline (Eq. 6). The use of wave energy
 337 implies the assumption of single-period waves.

$$338 \quad \frac{dx}{dt} = k_{wave} E, \quad (4)$$

$$339 \quad E = \frac{1}{16} \rho g H^2 \cos(\varphi - \theta), \quad (5)$$

$$340 \quad E \propto \rho g F \cos(\varphi - \theta), \quad (6)$$

341 The strength loss of a cell due to waves can be described as

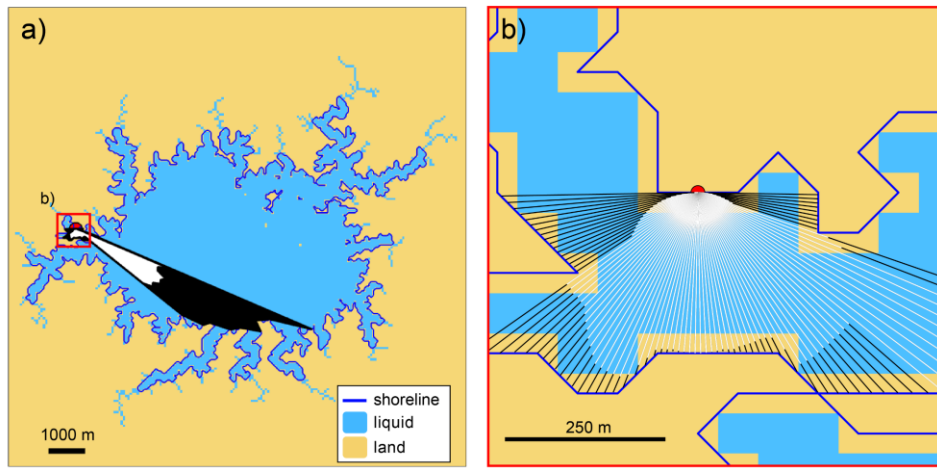
$$342 \quad \frac{\Delta S_{ij}}{S_0} = -k_{wave} \left(s_c + \frac{\sqrt{2}c}{2} \right) \int_{\varphi=0}^{2\pi} F(\varphi) \cos(\varphi - \theta) d\varphi \frac{\Delta x}{\Delta x_0} \Delta t. \quad (7)$$

343 If the strength loss in a time step exceeds a parameter-set threshold, a sub-timestep
 344 routine is implemented. Because the fetch calculation is the costliest step of the model, in this
 345 sub-timestep routine, we estimate the fetch weighting by interpolating the fetch of the nearest
 346 neighbor shoreline cells. This avoids additional costly fetch computations during the sub-
 347 timestep updates and allows us to approximate erosion driven by waves in a way that limits error
 348 without slowing down the model simulation.

349 3.3.1 Modeling wave energy density

350 The rate of strength loss of each shoreline cell is proportional to the wave energy density.
351 We model the wave energy density to be proportional to the fetch and the cosine of the angle
352 between the incident wave crest and the shoreline (~~Fig. 4~~Fig. 5). To compute this quantity, we
353 measure the fetch in all directions around the shoreline, in increments of $d\varphi$, for each shoreline
354 cell. For each direction, we extend a ray from the cell center in the direction $90^\circ - \varphi$ and step
355 along the ray in increments of a distance δ until reaching the opposite shore. This modeling
356 approach does not consider the effects of shoaling or refraction, so waves that would approach
357 from beyond 90° are not considered. When the ray extends past the opposite shoreline, we take
358 one step back and define this point as the intersection. The distance between this intersection and
359 the originating shoreline cell center is the fetch in the direction from which a wave would
360 propagate (Fig 4b). The length of fetch may be truncated at an input maximum length which
361 would represent the distance at which waves saturate and do not continue to grow. To calculate
362 the amount of strength loss each cell incurs, we compute the area of a polygon defined by the
363 ray-shoreline intersections for that cell (~~Fig. 4~~Fig. 5a). We call this area the “fetch area.” The
364 length of the ray in each direction is then weighted by the cosine of the angle between the
365 shoreline and the incident wave crest, $\varphi - \theta$ (~~Fig. 4~~Fig. 5a). The area of the polygon defined by
366 these cosine-weighted fetch lengths is computed and called the “wave area.” The wave area for
367 each point on the shoreline approximates the integral in Eq. 7.

368

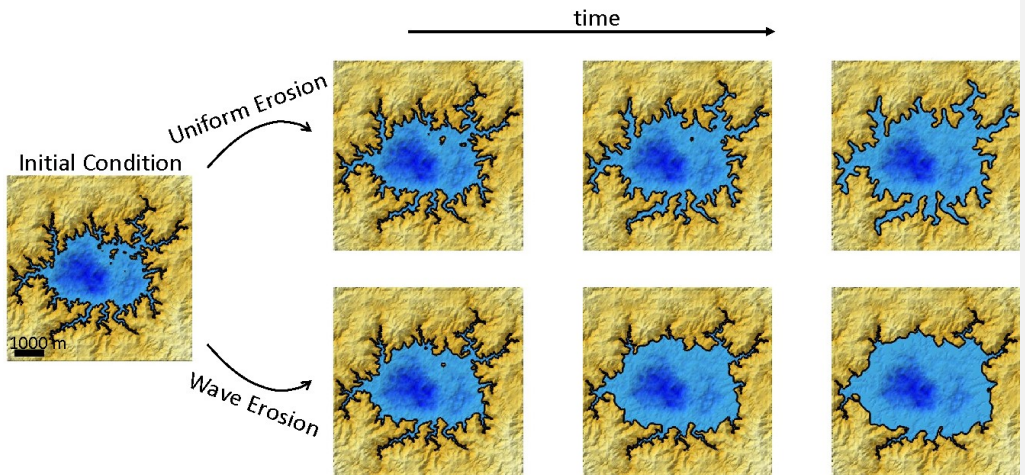


369

370 Figure 54: a) Fetch area (black) and wave area (white) computed for a point (red circle) on a
371 typical model shoreline (blue). The area shown in b) is outlined in red. b) Zoomed-in view of
372 fetch line-of-sight rays (black) and angle-weighted line-of-sight rays (white) computed for the
373 same point. In this example, $d\phi = 2^\circ$ and the ray step size, $\delta = 0.05$ m.

374 3.4 Model output

375 The model can be initialized with any user defined topographic model. In the simulations
 376 presented here, we initialize the grid with a synthetic topography consisting of a pseudo-fractal
 377 surface with variance of 10,000 superimposed on an elliptical depression with a depth of 25% of
 378 the domain relief and eroded by river incision to 95% of the initial terrain relief using a
 379 landscape evolution model (Perron et al., 2008, 2009, 2012). We then flood the domain by
 380 raising ~~sea or lake~~ level by 40 m. The model of shoreline retreat by uniform and wave erosion
 381 is then applied to the domain. Here, we show examples of an initial landscape eroded by either
 382 wave erosion or uniform erosion, to illustrate separately the effects of the two erosional
 383 mechanisms in the model (Fig. 5Fig. 6). However, all model components may be run in
 384 combination. We do not provide examples of combined uniform and wave erosion models here.
 385 The initial shoreline exhibits a dendritic shape due to flooding of the incised river valleys
 386 (Fig. 5Fig. 6). Through time, the uniform erosion model drives shoreline retreat at the same rate
 387 everywhere around the perimeter of the lake, resulting in widening valleys and increasing the
 388 pointedness of promontories or headlands (Fig. 5Fig. 6). The overall shape of the lake is
 389 maintained, but becomes smoother and tends toward circular. In the case of wave erosion, the
 390 river valleys erode slowly while the exposed parts of the coast erode more rapidly (Fig. 5Fig. 6).
 391 The embayed river valleys largely maintain their shapes, whereas the central, high-fetch portion
 392 of the ~~lake coast~~ grows larger and smoother.



393 Figure 65: Shaded relief maps of example model simulations of uniform erosion and wave
 394 erosion through time, starting from the same initial condition. Blue color indicates liquid cells,
 395 with darker blues indicating deeper depths. Gold color indicates land cells, with lighter shades
 396 indicating higher elevations. Black lines trace shorelines. Erodibility coefficients are $k_{wave} =$
 397 $k_{uniform} = 0.00001 \text{ m}\cdot\text{yr}^{-1}$. Uniform erosion (top) results in greater overall smoothness that is
 398 punctuated by pointy headlands, whereas wave erosion (bottom) results in blunted headlands,
 399 smooth open sections of coast, and preservation of sharp features in sheltered areas. Landscape
 400

401 time-steps shown correspond to similar amounts of erosion between wave and uniform
402 examples. The shoreline is defined as 4-connected in these examples.

403 To test our model performance, we compare the planform morphologies of model output
404 with example shorelines that have known geomorphic processes. While long term coastal cliff
405 retreat rates could be determined using dating techniques at local field sites (Hurst et al., 2016;
406 Bossis et al., 2024), more detailed testing of the model would require recreation of plan-view
407 shape at a broader scale. Because ~~the~~ long-term changes in planform morphology during retreat
408 of bedrock coastlines ~~are~~ generally too slow to be measurable with historical aerial and satellite
409 images, the data needed to fully validate this model are not presently available. Nonetheless, a
410 visual comparison can be drawn between coastal features found on Earth and the coastline
411 shapes generated by each end-member erosional mechanism in the model, which is the main goal
412 of our modeling approach. ~~Instances of dissolution and backwasting include karst lakes found in~~
413 the Plitvice Lakes, Croatia (Fig. 6d) and in Florida, USA (Fig. 6a) as well as ~~searp retreat due to~~
414 weathering and backwasting, such as Caineville Mesa, Utah, USA (Fig. 6b). These shorelines
415 exhibit the same overall smoothness, punctuated by sharp headlands, as is seen in the shorelines
416 formed by uniform erosion in our model (Fig. 5Fig. 6). ~~And a~~ Although it is beyond the scope of
417 this paper, output from this model could be used to quantitatively describe shoreline morphologic
418 differences~~y~~ driven by wave and uniform erosional processes or signatures of sea- or lake- level
419 changes.

420 A bedrock lake that has been eroded recently by waves is exemplified by Lake Rotoehu,
421 New Zealand (Fig. 6Fig. 7c). In these examples, we observe blunted headlands and smooth,
422 rounded stretches in open sections of coast, and crenulated shorelines in more protected areas of
423 coast – similar to the shorelines formed by wave erosion in our model (Fig. 5Fig. 6).

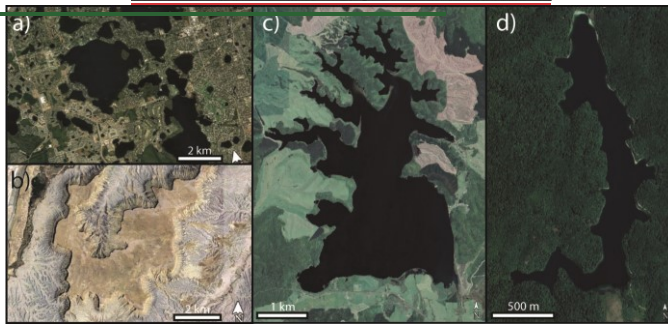
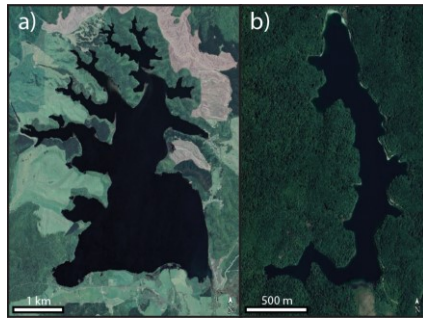


Figure 6: a) Karst lakes in Florida, USA (Map Data: © Google Earth, Landsat/Copernicus). Lake Butler and the surrounding region. b) Caineville Mesa, Utah, USA (Map Data: © Google Earth, Landsat/Copernicus). Figure 7: a) Lake Rotoehu, New Zealand (Map Data: © Google Earth, CNS/Airbus). b) Plitvice Lakes, Croatia (Map Data: © Google Earth, DigitalGlobe).

4 Model tests

4.1 Comparison with analytical solution and sensitivity to shoreline connectedness

For the simple case of an initially circular shoreline, we compute the shoreline evolution analytically and compare this known solution with our numerical model results. For the uniform erosion case, the rate at which the radius of a circle increases, \dot{r} , is equal to the constant of erosion, in this case $k_{uniform}$.

$$\dot{r}(t) = k_{uniform} \quad (8)$$

Therefore, the radius, r , at time, t , and initial radius, r_0 , for uniform erosion is:

$$r(t) = r_0 + k_{uniform}t \quad (9)$$

For wave erosion, the rate of increase of the radius, \dot{r} , depends on the constant of erosion, k_{wave} , and the integral of the fetch, F , at each angle between the incoming wave crest and the shoreline, $(\varphi - \theta)$ in all directions around the circle:

445
$$F(\varphi) = r\sqrt{2(1 + \cos(2(\varphi - \theta)))}$$
 (10)

446
$$\dot{r}(t) = \frac{k_{wave}}{2} \int_{-\frac{\pi}{2}}^{\frac{\pi}{2}} (F(\varphi) \cos(\varphi - \theta))^2 d\varphi$$
 (11)

447 Computing this integral simplifies to:

448
$$\dot{r}(t) = k_{wave} \frac{3\pi}{4} r(t)^2$$
 (12)

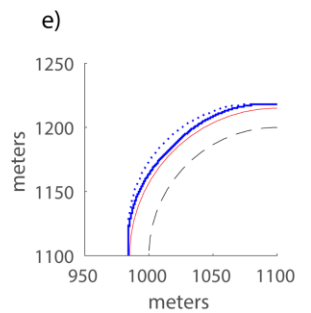
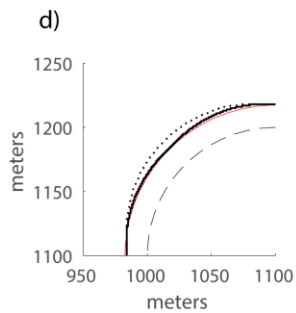
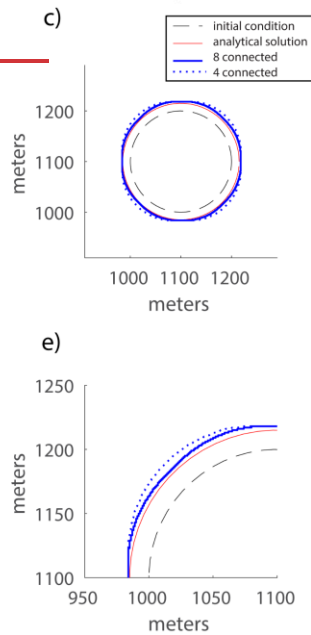
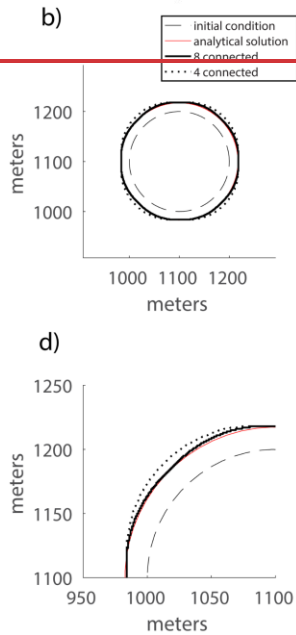
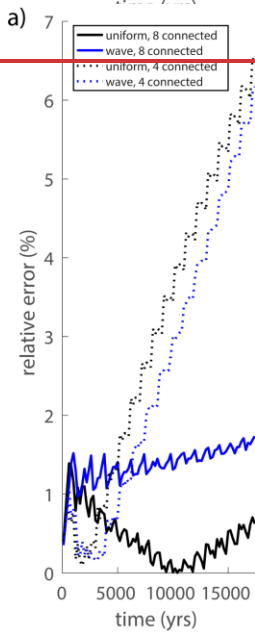
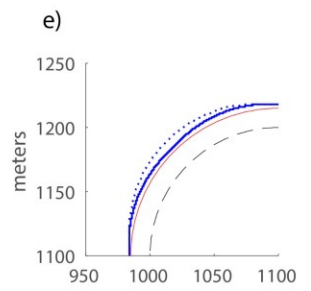
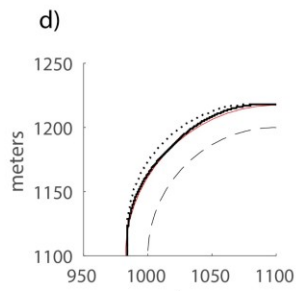
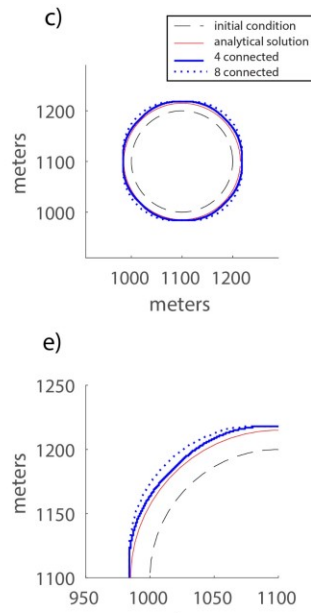
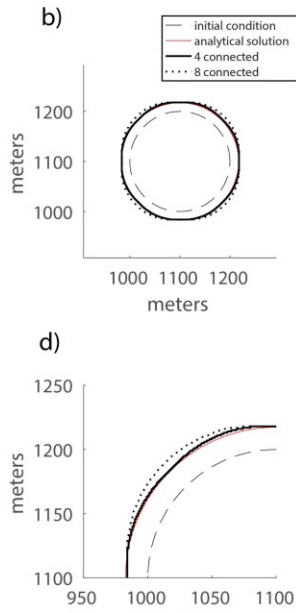
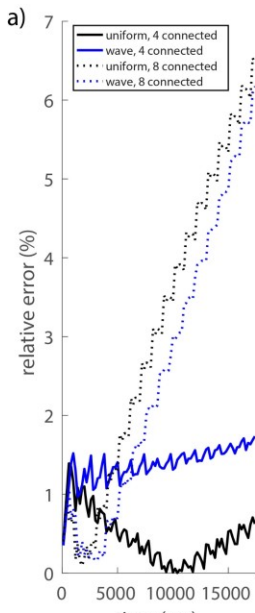
449 Therefore, the radius, r , at time, t , for wave erosion is:

450
$$r(t) = \frac{r_0}{1 - r_0 k_{wave} \frac{3\pi}{4} t}$$
 (13)

451 We use the analytical solution for the radius through time for each case to calculate the
 452 shoreline position and area of the circular lake as it is eroded by either uniform or wave erosion.
 453 To compute the relative error of the numerical model, a test circular lake is eroded for 17,400
 454 years, resulting in approximately 20% and 25% increase in lake area for wave and uniform
 455 erosion, respectively, and compare this to the analytical solution.

456 Because the model operates on a rectangular grid, some amount of distortion of a circle is
 457 expected. While this distortion cannot be avoided entirely by increasing the grid resolution,
 458 increasing it can reduce the error in the shoreline shape by allowing the shoreline to retreat in
 459 finer increments. A fine grid, however, comes at increased computational cost. The spatial
 460 resolution, Δx and Δy , should be chosen to be small enough to represent the features of the
 461 shoreline, but large enough to keep computational costs reasonable.

462 We perform these simulations for uniform and wave erosion with both ~~48~~-connected and
 463 ~~84~~-connected versions of the model (Fig. 3 Fig. 4). The ~~48~~-connected model performs
 464 significantly better than the ~~84~~-connected model, as shown by the relative error in lake area. The
 465 ~~48~~-connected case maintains relative error less than 2% throughout the simulation whereas the
 466 error in the ~~84~~-connected model increases roughly linearly with time, ending at approximately
 467 7% (Fig. 7a). The distortion is worse in the ~~84~~-connected case for both uniform erosion and wave
 468 erosion, and systematically worse in the diagonal directions (Fig. 7b,c). This analysis suggests
 469 that grid bias is a more important source of error in the model than spatial discretization.



472 Figure 7: a) The error in lake area through time of an initially circular lake relative to the
473 analytical solution for 48-connected (solid) and 84-connected (dotted) models of uniform erosion
474 (black) and wave erosion (blue). The initial condition (dashed), analytical solution (red), and
475 modeled 48-connected and 84-connected shorelines at time=17400 are shown for b) uniform
476 erosion and c) wave erosion, with zoomed in results shown for d) uniform erosion and e) wave
477 erosion.

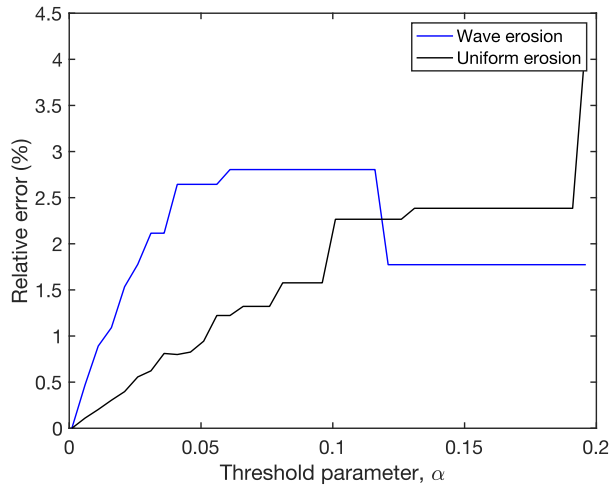
478 4.2 Resolution sensitivity

479 4.2.1 Grid resolution

480 Although the grid resolution affects the size of the features that can be resolved in the
481 landscape, it does not substantially affect the amount of coastal erosion. As discussed above, the
482 strength loss in this model is insensitive to grid resolution, Δx , and time step, Δt , assuming that
483 Δx is fine enough to resolve the features of interest and that Δt is small enough to limit erosion
484 to less than the maximum cell strength in a single time step. The total amount of strength in the
485 domain is independent of Δx because the number of cells is proportional to Δx^{-2} and the
486 strength of each cell is proportional to Δx^2 . The damage in each time step is independent of Δx
487 because the number of cells on the shoreline is proportional to Δx^{-1} and the damage per cell is
488 proportional to Δx .

489 4.2.2 Threshold strength parameter

490 The threshold strength parameter, α , was introduced to prevent excess strength reduction
491 from being neglected when a cell has less strength than is depleted in a timestep. A smaller
492 threshold strength parameter results in a more frequent application of the sub-timestep routine
493 and smaller sub-timesteps. With a less stringent threshold strength parameter (>0.05), the
494 shoreline may erode more than the analytical solution in a time step, leading to a positive slope
495 in the relative error in strength against the threshold strength parameter (Fig. 8).

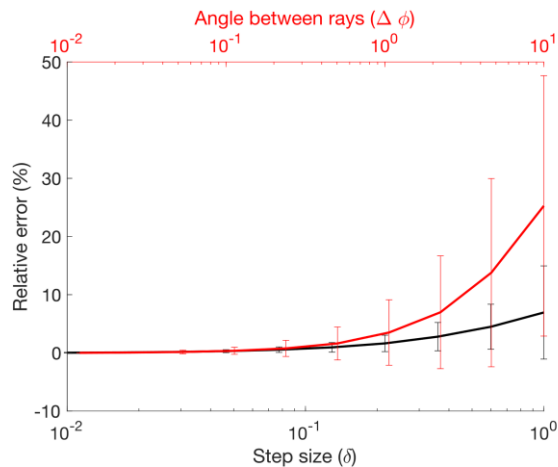


496
 497 Figure 8: Error in total strength reduction as a function of the threshold strength parameter,
 498 expressed as a percentage of the error for the smallest value of the threshold strength parameter,
 499 for a typical model lake (the initial condition in Fig. 5 Fig. 6) eroded over one time step by
 500 uniform erosion (black) and wave erosion (blue).

501 4.3 Fetch ray angular and distance increments

502 We test the sensitivity of the fetch-area calculation to the angle between rays, $d\phi$, and the
 503 ray step size, δ . This test allows us to analyze the error in fetch of a typical model due to these
 504 parameters. The error measurements provide a basis for selecting an angle between rays and a
 505 ray step size that optimize the trade between computational time and model accuracy.

506 We compute the error in fetch area over a range of ray angles and step sizes. With a fixed
 507 ray step size of $0.05\Delta x$ (the nominal step sized used in our simulations), we compute the fetch
 508 error for each shoreline cell over a range of 0.012° to 10° , corresponding to 30,000 and 36 rays,
 509 respectively. With a fixed ray angle of 2° (the nominal ray angle used in our simulations), we
 510 compute the relative fetch error over a range of ray step sizes between $0.01\Delta x$ to Δx . The fetch-
 511 area error of each cell is computed relative to the fetch area of the finest resolution in each
 512 parameter: 2° between rays and a ray step size of $0.05\Delta x$ (Fig. 9). The error, as well as the
 513 standard deviation in errors, in each scenario converges to zero, indicating that as the angle
 514 between rays and the ray step size become small the fetch area converges to a constant value.



515
516 Figure 9: Relative error in fetch area for a range of step sizes with ray angle of 2° (black) and for
517 a range of ray angles with step size of $0.05\Delta x$ (red).

518 5 Discussion and Conclusions

519 In this paper, we present NEWTS1.0, a cellular model of coastline erosion in detachment-
520 limited environments by uniform erosion and by wave erosion. For uniform erosion, the
521 coastline erodes at a constant rate everywhere along the shoreline. For wave-driven erosion, the
522 coastline erodes as a function of the fetch and the angle between the incident waves and the
523 shoreline.

524 While our uniform erosion rate law is similar to that of Howard (1995), our modeling
525 approach is different. Because there are multiple mechanisms that may erode a coast in our
526 model, memory of the strength loss of the substrate is necessary. Rather than rays extending at a
527 constant rate from the interior points representing retreat as is done in Howard's 1995 model, the
528 strength of shoreline (or scarp edge) points is reduced by an amount proportional to the number
529 and direction of neighboring lake cells.

530 Our wave erosion model contains a dependence on wave ~~power-energy~~ like in other
531 models (Walkden and Hall, 2005; Limber et al., 2014), but simplifies the influence of sediment
532 and other factors to a constant. This simplification is useful for locations without readily
533 available grain size or sediment cover data, and to investigate the long-term influence of these
534 processes. However, a limitation of this simplified approach is the implicit assumption of a
535 singular single wave period when using wave energy rather than wave power for in the wave
536 erosion rate law (Equations 4-6). Future work could extend the capabilities to include
537 consideration of wave period.

538 Our model is also unusual among coastal erosion models in that it evaluates multiple
539 closed coastlines (or lakes) in a landscape domain rather than a single reach of open coastline,
540 and that it focuses on the planform morphology of eroding rocky closed-basin shorelines. A
541 limitation of this model is that sediment redistribution is not included in the erosion rate laws and
542 there is no sedimentation along the coast. Sediment abrasion and cover could be incorporated in

Formatted: Space After: 0 pt

543 future versions of our model through a spatially heterogeneous and time-dependent erodibility
544 coefficient, k ; however, this would likely require parameterization from field data.

545 While this model is currently configured to simulate the erosion of closed basins, such as
546 lakes or inland seas, modifications could be made to evaluate open stretches of coast. The two
547 routines that would need to be considered are the routines to order the shoreline and to compute
548 fetch. The routine to ordering the shoreline routine requires that the shoreline be a closed loop.
549 To evaluate an open stretch of coast in the model, either the landscape domain could be modified
550 to artificially enclose the open coast or the boundary conditions. The simpler approach is to
551 modify the landscape domain ~~could be modified~~ such that an artificial and large basin was made
552 surrounding the domain, identifying these as fixed points that do not erode, and making sure the
553 modified landscape is further than the fetch saturation length from the shoreline of interest. To
554 evaluate an ocean island, enclose it in land beyond the fetch saturation length in distance from
555 the island. If the domain is modified such that the shoreline is a closed loop, all routines should
556 function appropriately. However, if a different routine to order the shoreline is used, the fetch
557 computation would need to be slightly modified. Currently, fetch is computed as an extended ray
558 from a shoreline cell that advances at some interval length until it reaches land and allows for a
559 fetch threshold at some length of wave saturation (See Section 3.3.1). The truncation of
560 computed fetch at the threshold length is implemented following the calculation of the fetch
561 length. If there isn't land on the opposite side of the ray, an error would occur. Therefore, by
562 truncating the fetch length as the ray is extending rather than after the opposite land is found,
563 fetch could be calculated for open coasts. A more complicated, but preferable approach would be
564 to change the boundary conditions. If the boundaries of the open stretch of coast were periodic,
565 the entire coast could retreat without introducing an artificial boundary edge and a larger domain.
566 The shoreline would be "closed" when it crosses the periodic boundary and arrives at the
567 repeated point. If a fetch vector went off the periodic boundary, it would wrap around to the
568 other side and continues. If a periodic boundary condition is deemed inappropriate, a mirrored
569 boundary could be used instead. The shape of the coast would be reflected in each boundary, and
570 fetch vectors would reflect off the boundary. However, this change to the fetch computation is
571 unnecessary if the domain is modified such that the order the shoreline routine is upheld.

572 As a reduced-complexity model, NEWTS1.0 can be applied to investigate coastal
573 systems in remote environments where field work is difficult or impossible. This includes
574 locations such as the arctic or Saturn's moon Titan, home to the only other active coastlines in
575 our solar system. The simplicity of our model allows for efficient, long-term simulations of
576 coupled landscape evolution and coastal erosion in detachment-limited systems. Among coastal
577 systems on Earth, investigations of fetch dependence and the resulting morphology given a
578 combination of erosional mechanisms would be particularly relevant to the carbonate
579 geomorphology community, as dissolution and wave activity are both often acting
580 simultaneously along these coasts.

581 **Acknowledgments**

582 We thank David Mohrig, Di Jin, Heidi Nepf, Jorge Lorenzo-Trueba, Santiago Benavides,
583 and Paul Corlies for helpful discussions. Any use of trade, firm, or product names is for
584 descriptive purposes only and does not imply endorsement by the U.S. Government.

585 **Funding:**

586 National Science Foundation Graduate Research Fellowship grant 1745302 (RVP)
587
588

Formatted: Space After: 0 pt

589 NASA Cassini Data Analysis Program grants 80NSSC18K1057 and 80NSSC20K0484
590 (RVP, JTP, ADA, JMS, SPDB, AGH).
591 United States Geological Survey, Coastal and Marine Hazards Research Program (RVP)
592 Heising-Simons Foundation (SPDB)
593

594 **Author contributions:**

595 Conceptualization: RVP, JTP, ADA, JMS, SPDB, AGH
596 Methodology: RVP, JTP, ADA, JMS
597 Investigation: RVP, JTP, ADA
598 Visualization: RVP
599 Supervision: JTP, ADA, AGH
600 Writing—original draft: RVP
601 Writing—review & editing: RVP, JTP, ADA, JMS, SPDB, AGH
602

603 **Competing interests:** Authors declare that they have no competing interests.
604

605 **Code/Data availability:** NEWTS1.0 model (Palermo et al., 2023) code is available at
606 <https://doi.org/10.5066/P9Q6GDGP>.
607
608

609 **6 References**

- 610 Adams, P.N., 2004, Assessing coastal wave energy and the geomorphic evolution of rocky coasts
611 [Ph.D. thesis]: Santa Cruz, California, University of California–Santa Cruz, 175 p.
612 Adams, P.N., Anderson, R.S., and Revenaugh, J., 2002. Microseismic measurement of wave
613 energy delivery to a rocky coast: *Geology*, v. 30, p. 895–898, doi:10.1130/0091-
614 7613(2002)030 <0895:MMOWED>2.0.CO;2.
615 Adams, P.N., Storlazzi, C.D., Anderson, R.S., 2005. Nearshore wave-induced cyclical flexing of
616 sea cliffs. *Journal of Geophysical Research Earth Surface* 110, 1–19,
617 <https://doi.org/10.1029/2004JF000217>.
618 Ashton, A. D., Murray, A. B., Littlewood, R., Lewis, D. A., & Hong, P., 2009. Fetch-limited
619 self-organization of elongate water bodies. *Geology*, 37(2), 187-190.
620 [Bossis, R., Regard, V., Carretier, S., & Choy, S. \(2024\). Evidence of slow millennial cliff retreat](#)
621 [rates using cosmogenic nuclides in coastal colluvium. *EGUsphere* \[preprint\], 2024, 1-15.](#)
622 Bramante, J. F., Perron, J. T., Ashton, A. D., and Donnelly, J. P., 2020. Experimental
623 quantification of bedrock abrasion under oscillatory flow, *Geology*, 48, 541–545,
624 <https://doi.org/10.1130/G47089.1>.
625 Emery, K. O., and Kuhn, G. G., 1980. Erosion of rock coasts at La Jolla, California. *Marine*
626 *Geology*, 37, 197–208.
627 [Esri. "Imagery" \[basemap\]. 1:365,662. "World Imagery". January 18, 2024.](#)
628 <https://www.arcgis.com/home/item.html?id=10df2279f9684e4a9f6a7f08febac2a9>. (Jan
629 [31, 2024](#)).630 Günther, F., Overduin, P.P., Sandakov, A.V., Grosse, G., Grigoriev, M.N., 2013. Short and long-
631 term thermo-erosion of ice-rich permafrost coasts in the Laptev Sea region.
632 *Biogeosciences* 10, 4297–4318.

- 633 Hasselmann, K., Barnett, T.P., Bouws, E., Carlson, H., Cartwright, D.E., Enke, K., Ewing, J.A.,
634 Gienapp, A., Hasselmann, D.E., Kruseman, P. and Meerburg, A., 1973. Measurements of
635 wind-wave growth and swell decay during the Joint North Sea Wave Project
636 (JONSWAP). *Ergaenzungsheft zur Deutschen Hydrographischen Zeitschrift, Reihe A*.
637 Howard A. D. (1995) Simulation modeling and statistical classification of escarpment planforms.
638 *Geomorphology* 12.3, 187–214, 61–78.
639 Huppert, K. L., Perron, J. T., & Ashton, A. D., 2020. The influence of wave power on bedrock
640 sea-cliff erosion in the Hawaiian Islands. *Geology*, 48(5), 499-503.
641 <https://doi.org/10.1130/G47113.1>
642 [Hurst, M. D., Rood, D. H., Ellis, M. A., Anderson, R. S., & Dornbusch, U., 2016. Recent](#)
643 [acceleration in coastal cliff retreat rates on the south coast of Great Britain. *Proceedings*](#)
644 [of the National Academy of Sciences, 113\(47\), 13336-13341.](#)
645 Kline, S.W., Adams, P.N., Limber, P.W., 2014. The unsteady nature of sea cliff retreat due to
646 mechanical abrasion, failure and comminution feedbacks. *Geomorphology* 219, 53–67,
647 <https://doi.org/10.1016/j.geomorph.2014.03.037>.
648 Komar P. D., 1998. Prentice-Hall, Englewood Cliffs, New Jersey, 429 pp.
649 Lamont-Smith T, Waseda T., 2008. Wind Wave Growth at Short Fetch. *Journal of Physical*
650 *Oceanography*, 38(7), 1597-1606. doi:10.1175/2007JPO3712.1
651 Limber, P.W., Murray, A.B., Adams, P.N., Goldstein, E.B., 2014. Unraveling the dynamics that
652 scale cross-shore headland relief on rocky coastlines: 1. Model development. *Journal of*
653 *Geophysical Research Earth Surface* 119, 854–873,
654 <https://doi.org/10.1002/2013jf002950>.
655 Limber, P.W., Murray, A.B., 2011. Beach and sea-cliff dynamics as a driver of long-term rocky
656 coastline evolution and stability. *Geology* 39, 1147–1150,
657 <https://doi.org/10.1130/g32315.1>.
658 Palermo, R. V., Piliouras, A., Swanson, T. E., Ashton, A. D., & Mohrig, D., 2021. The effects of
659 storms and a transient sandy veneer on the interannual planform evolution of a low-relief
660 coastal cliff and shore platform at Sargent Beach, Texas, USA. *Earth Surface Dynamics*,
661 9(5), 1111-1123.
662 Palermo, R.V., Perron, J.T., Soderblom, J.M., Birch, S.P.D., Hayes, A.G., Ashton, A.D., 2023,
663 Numerical model of coastal Erosion by Waves and Transgressive Scarps (NEWTS)
664 Version 1.0: U.S. Geological Survey software release,
665 <https://doi.org/10.5066/P9Q6GDGP>.
666 Perron, J. T., Dietrich, W. E., & Kirchner, J. W., 2008. Controls on the spacing of first-order
667 valleys. *Journal of Geophysical Research: Earth Surface*, 113(4), 1–21.
668 <https://doi.org/10.1029/2007JF000977>
669 Perron, J. T., J. W. Kirchner, and W. E. Dietrich, 2009. Formation of evenly spaced ridges and
670 valleys, *Nature*, 460, 502–505, doi:10.1038/nature08174.
671 Perron, J. T., P. W. Richardson, K. L. Ferrier, and M. Lapôte, 2012. The root of branching river
672 networks, *Nature*, 492, 100–103, doi:10.1038/nature11672.
673 Ranasinghe, R., 2020. On the need for a new generation of coastal change models for the 21st
674 century. *Scientific reports*, 10(1), p.2010.
675 Robinson, L. A., 1977. Marine erosive processes at the cliff foot, *Marine Geology*, 23, 257–271,
676 [https://doi.org/10.1016/0025-8532\(77\)90022-6](https://doi.org/10.1016/0025-8532(77)90022-6).

Formatted: Italian (Italy)

677 Sunamura, T. (2018). A fundamental equation for describing the rate of bedrock erosion by
678 sediment-laden fluid flows in fluvial, coastal, and aeolian environments. *Earth Surface*
679 *Processes and Landforms*, 43(15), 3022-3041.

680 Sunamura, T., 1976. Feedback relationship in wave erosion of laboratory rocky coast, *The*
681 *Journal of Geology*, 84, 427–437, 115 <https://doi.org/10.1086/628209>.

682 Sunamura, T., 1992. *Geomorphology of Rocky Coasts*. Wiley, Chichester, UK.

683 Trenhaile, A. S., 1987. *The Geomorphology of Rock Coasts*, Oxford University Press, Oxford.

684 Trenhaile, A.S., 2001. Modeling the effect of weathering on the evolution and morphology of
685 shore platforms. *Journal of Coastal Research*, 17, 398–406.

686 Trenhaile, A. S., 2002. Rock coasts, with particular emphasis on shore platforms,
687 *Geomorphology*, 48, 7–22, [https://doi.org/10.1016/S0169-555X\(02\)00173-3](https://doi.org/10.1016/S0169-555X(02)00173-3).

688 Trenhaile, A.S., 2011. Cliffs and Rock Coasts. In: *Treatise on Estuarine and Coastal Science*
689 Vol. 3, eds. Flemming, B.W. and Hansom, J.D., Elsevier, p. 171-192

690 Trenhaile AS., 2015. Coastal notches: Their morphology, formation, and function. *Earth-Science*
691 *Reviews*. 150, 285-304. doi:10.1016/j.earscirev.2015.08.003

692 Trenhaile, A.S., 2016. Rocky coasts—Their role as depositional environments. *Earth-Science*
693 *Reviews*. 159, 1–13.

694 Walkden, M. J. A. and Hall, J. W., 2005. A predictive Mesoscale model of the erosion and
695 profile development of soft rock shores, *Coastal Engineering*, 52, 535–563, 20
696 <https://doi.org/10.1016/j.coastaleng.2005.02.005>.

697 Young, A. P., R. E. Flick, W. C. O’Reilly, D. B. Chadwick, W. C. Crampton, and J. J. Helly,
698 2014. Estimating cliff retreat in southern California considering sea level rise using a
699 sand balance approach, *Marine Geology*, 348,15–26,
700 <https://doi.org/10.1016/j.margeo.2013.11.007>.